Int. J. Electrochem. Sci., 11 **(2016)** 3664 - 3679

International Journal of
ELECTROCHEMICAL
SCIENCE
www.electrochemsci.org

Monitor the Adsorption of Bromine Vapor on Zeolitic-Imidazolate Framework-8 Film by an Electrodeless Quartz Crystal Microbalance in Overtone

Dazhong Shen[*], *Lingqiang Kong, Xiaolong Ma, Xuxiang Wang, Honghai Wang, Qi Kang*[*]

College of Chemistry, Chemical Engineering and Materials Science, Collaborative Innovation Center of Functionalized Probes for Chemical Imaging in Universities of Shandong, Key Laboratory of Molecular and Nano Probes, Ministry of Education, Shandong Provincial Key Laboratory of Clean Production of Fine Chemicals, Shandong Normal University, Jinan 250014, P. R. China.
[*]E-mail: dzshen@sdnu.edu.cn; qikang@sdu.edu.cn

Received: 10 January 2016 / *Accepted:* 28 January 2016 / *Published:* 1 April 2016

In this work, the overtone response of an electrodeless quartz crystal microbalance (EL-QCM) in gaseous phase was investigated by an impedance analysis method. It was shown that the influence of the electrode gap on the resonant frequency reduces with increasing overtone number. Although reduced with increasing overtone, the effective quality factor is still high enough even at 7th overtone (3.8 ± 10^4) for the stable resonance of the EL-QCM. The EL-QCM was applied to monitor the adsorption processes related to corrosive gas, modeling by bromine vapor onto zeolitic-imidazolate framework-8 (ZIF-8) film. It was shown that the 2-methylimidazole unit in ZIF-8 plays important role for Br_2 adsorption, preponderating in chemical adsorption. The adsorption kinetic data are in agreement with the pseudo-second-order model. The adsorption isotherms are well fitted by the Langmuir model with the saturation adsorption capacity of 3241 mg/g on ZIF-8 with thickness of 0.699 μm (25°C). The correlations of the frequency shifts at the overtone (n=1,3,5) can be employed to judge the rigidity of the film in an adsorption process.

Keywords: Quartz crystal microbalance; Electrodeless; Overtone response; Bromine adsorption; Zeolitic-imidazolate framework

1. INTRODUCTION

The quartz crystal microbalance (QCM) technique, operating based on the piezoelectric properties of quartz crystals, is a powerful tool for the real-time characterization and quantification of molecular interactions, since it provides label-free and on-line analysis [1]. It has been successfully demonstrated the applications of the QCM in electrochemistry [2,3], solution chemistry[4,5] and

doi: 10.20964/110352

biosensors [7-11]. Usually, a QCM sensor is constructed with an AT-cut piezoelectric quartz crystal (quartz wafer) disc sandwiched between two metal film electrodes, which induce the quartz crystal to oscillate at a frequency in the MHz. The sensitive area of a QCM is limited to the crossed area between the electrodes. Sauerbrey described that the shift in frequency is related to the change in mass [12], hence adsorbed or desorbed matter changes the oscillation frequency, Δf, of the sensor crystal. When an ultrathin, homogeneous and rigid mass loading is deposited on the electrode surface, as seen in the Sauerbrey equation below, the adsorbed mass (Δm) is in a linear correlation to □

$$\Delta f = -2.26\times10^{-6} f_0^2 \frac{\Delta m}{A} \qquad (1)$$

where f_0 and A are the fundamental frequency and the electrode area of the QCM, respectively.

In the applications of QCM, the frequency stability and lifetime of a QCM depend greatly on the chemical stability of the electrodes. If the electrodes are eroded in a corrosive condition, the drift in the resonant frequency results in a large error in the measurement of mass change. On the other hand, the electrodes deteriorate the mass sensitivity because of much higher mass density of gold than that of quartz, and this influence becomes marked as the fundamental resonance frequency increases.[13] Such disadvantages can be overcome by using a kind of electrodeless quartz crystal microbalance (EL-QCM) [14,15]. The applications of the EL-QCM sensors in adsorption [16,17], electroless plating [18], lipid bilayer [19], and biosensors [20-22] were reported. Recently, EL-QCM in gaseous phase was integrated with UV/Vis spectroscopy for the investigation of the photodecomposition of methylene blue [23] .

In a previous paper, the response and equivalent circuit parameters of the EL-QCM in gaseous phase were measured by an impedance analysis method [24]. In the present work, an EL-QCM was applied to investigate the adsorption of bromine vapor, taking advantage of its excellent chemical stability. Zeolitic-imidazolate framework-8 (ZIF-8) film was chosen as the model sorbent because it is an excellent sorbent for molecular I_2 because of its suitable pore aperture size, large specific surface area, and high chemical and thermal stability [25,26]. Under our experimental conditions, ZIF-8 exhibits also high adsorption capacity to Br_2. It was shown that the motional resistance of the EL-QCM increases steeply in the case of high amount of Br_2 adsorbed. Hence, the overtone response of the EL-QCM in gaseous phase was investigated by an impedance analysis method. To our best knowledge, it is the first time to report the application of gaseous phase EL-QCM in overtone. The influence of the electrode gap on the resonant frequency and equivalent circuit parameters of the EL-QCM was investigated. The correlations of the frequency shifts in overtone (n=1,3,5) were used to indicate the change in rigidity of the film. The influence of the thickness of ZIF-8 film and temperature on the adsorption kinetics and isotherm was reported.

2. EXPERIMENTAL

2.1. Reagents and instrumentation

AT-cut quartz discs (with diameter of 14 mm and fundamental frequency of 5.032 MHz) were purchased from Beijing Chenjing Electronics Co., Ltd. (China). All chemicals used were of analytical

grade. Bromine, zinc nitrate and 2-methylimidazole (mIm) were purchased from Shanghai Aladdin Reagents Company (China). Methanol and acetone were purchased from Tianjin Wenda Chemicals Company (China). The purified water used in the experiments was ion-exchanged with a Milli-Q system (Millipore, Bedford, MA, USA).

A schematic representation of the configuration of the setup for measuring the equivalent circuit parameters of EL-QCM is illustrated in Fig.1A. Two copper electrodes (with diameter of 6.5 mm and in coaxial with the quartz wafer) were used as the excitation electrodes. A copper shielding plate with thickness of 1 mm was employed to suppress to the by-pass current between the electrodes. A bare quartz wafer was mounted in the hole with a diameter of 14.5 mm in the shielding plate. The distance between the upper electrode and quartz wafer was adjusted by a mechanism similar to a micrometer. The electrodes were connected to a precision impedance analyzer (Agilent 4294A) by coaxial-cables. The parasitic capacitance and inductance of the test fixture and leading wires were corrected in the calibration step prior to impedance measurements. A user program written in Visual Basic 6.0 was used to acquire and process the impedance data. The conductance was scanned separately in the resonant region of the EL-QCM in overtone models (n=1,3,5,7) and the motional parameters were calculated according to the same Butterworth–Van Dyke model as a normal quartz wafer resonator. The resonant frequencies of the EL-QCM were estimated according to the arithmetic reported previously [27]. The static capacitances of the EL-QCM were measured directly at the frequency regions beyond the resonance of the quartz wafer ($0.9nf_0 \pm 10$ kHz).

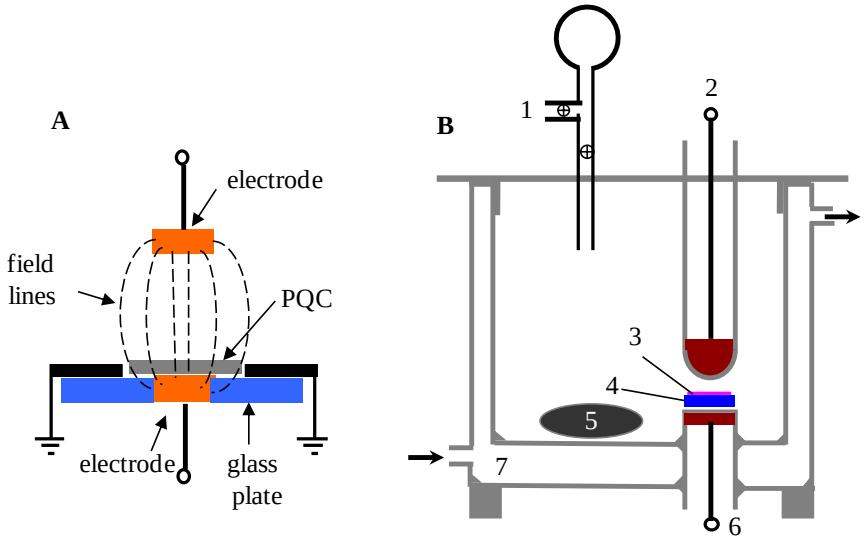

Figure1. Schematic drawing of experimental setups (not to scale) employed for equivalent circuit parameters (A) and adsorption measurements (B) .(1): inlet for adsorbate; (2) upper excitation electrode; (3): adsorbate film;(4): QCM sensor; (5): magnetic mixer; (6) bottom excitation electrode; (7): thermostatic water bath.

2.3 Monitoring adsorption of bromine on ZIF-8 film

To initiate film deposition, quartz discs were washed by chromosulfuric acid, water and acetone. After drying under a nitrogen flow, the quartz disc was mounted in the setup in Fig.1A with

an electrode gap of 1 mm. The resonant frequencies of the EL-QCM in overtone numbers (n=1,3,5) were recorded as the references. Then the quartz disc was mounted perpendicularly on a cell by two O-rings with one side facing the liquid phase. The growth of ZIF-8 film on the surface of quartz was started by adding a fresh mixture of 25 mM $Zn(NO_3)_2$ and 50 mM mIm in methanol into the cell. After 2h, the solution in the cell was replaced by a fresh mixture for next fabrication cycle until a ZIF-8 film of given thickness was grown. A group of quartz discs were mounted on the cell for batch growth of ZIF-8 film with similar thickness. The quartz discs with ZIF-8 film was rinsed by methanol and dried by a nitrogen flow. Afterwards, the resonant frequencies of the EL-QCM with ZIF-8 film were measured again in the same setup. The shift in the fundamental frequency model, ΔF_{01}, was calculated for estimation the thickness of ZIF-8 film (h) according to the Sauerbrey equation.

$$h = -\frac{4.43\times10^5 \Delta F_{01}}{\rho_f f_0^2} \qquad (2)$$

where ρ_f (= 0.95g/cm^3) is the density of ZIF-8 film [28].

The adsorption of bromine onto ZIF-8 film was monitored in the setup illustrated in Fig.1B. The responses in overtone numbers (n=1, 3, 5) of the EL-QCM were recorded in three separated impedance scans. Prior to adsorption, the cell was vacuumized until stable baselines were reached. A given volume of bromine was injected into the cell from the inlet and the adsorption process was started. A magnetic mixer was used to speed up the diffusion of the bromine vapor. The concentration of bromine was detected by a spectrometric method by using KI-starch solution. The changes in resonant frequency and motional resistance were recorded to estimate the mass adsorbed in real time. When the adsorbed layer behaves as a rigid solid, the areal mass is determined by the Sauerbrey equation. When the mass adsorbed approached to a plateau, the cell was vacuumized to measure the proportion of reversible adsorption. Then another volume of bromine vapor was injected for further adsorption at higher concentration of bromine.

All the adsorption experiments were performed thrice and the averaged values were reported.

3. RESULTS AND DISCUSSION

3.1 Overtone response of EL-QCM in gaseous phase

To eliminate electrode corrosion by Br_2 vapor, an EL-QCM is designed by using two separated-electrodes. The high frequency excitation voltage is applied on the quartz resonator by the conductance of the air and glass layers between the electrodes (Fig.1B). As deduced in a previous paper [24], the resonant frequency (F_0) of the El-QCM expressed by:

$$F_0 = f_0 + \frac{f_0 C_q}{2(C_0 + C_{air})} \qquad (3)$$

Where $f_0 = (2\pi\sqrt{L_q C_q})^{-1}$ is the fundamental resonant frequency of the bare quartz disc itself, C_q and C_0 are the static and motional capacitance of the quartz disc, respectively, C_{air} is the total series air capacitance between the electrodes.

Similar to a normal QCM, the overtone responses are also measurable in the EL-QCM. As illustrated in Fig.2, the intensity of the resonant peaks reduces while the width of the resonant peaks enlarges with increasing overtone number (n=1,3,5,7). Higher overtone number responses were not shown due to weaker intensity in conductance-frequency curve. For a normal 5 MHz QCM in vacuum, as reported by Cassiède and co-workers [29], the intensity of resonance in 3,5 and 7 overtones is 52.7%, 23.0% and 12.2% of that in fundamental frequency model, respectively. Under our experimental conditions, the intensity of resonance of the EL-QCM in 3,5 and 7 overtones is 34.3%, 16.5% and 10.9% of that in fundamental frequency model, respectively, which is less slightly than that in normal QCM. On the other hand, the half-bandhalf-width of the resonance in 1, 3,5 and 7 overtones is 33.6, 98.7, 275 and 436 Hz, respectively, which is similar with that in an normal 5 MHz QCM [29].

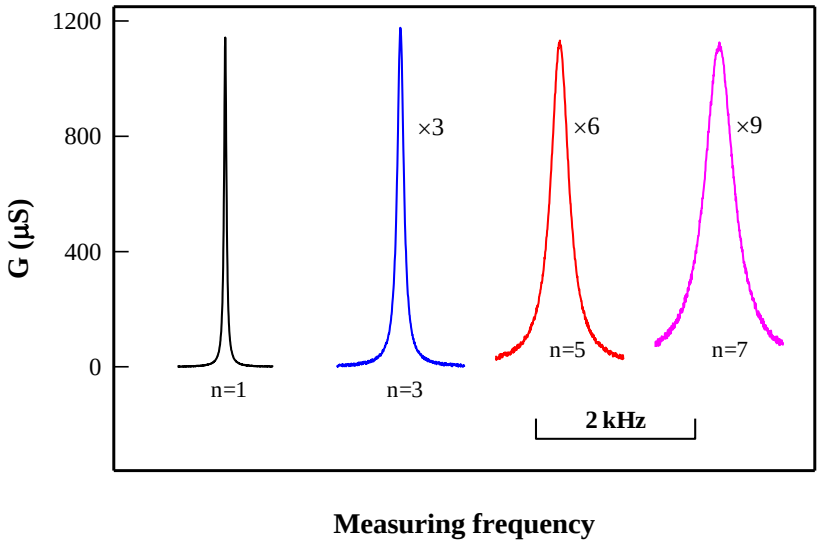

Figure 2. Conductance-frequency curves of EL-QCM in different overtone frequency region. The electrode gap was 2 mm.

Interestingly, as can be seen in Fig.3, the influence on the electrode gap on the resonant frequency of the EL-QCM (Fig.1A) is reduced with increasing overtone number. For example, with the gap increasing from 0.5 to 4.0 mm, the frequency shifts are 622, 219,139 and 98 Hz in the case of n=1,3,5,and 7, respectively. This is reasonable because the conductance of the air layer between the electrodes is expected to increase linearly with increasing frequency.

To explain the results further, the equivalent circuit parameters of the EL-QCM in the Butterworth–Van Dyke model were also measured and depicted in Fig.4. As deduced in a previous paper [24],the equivalent circuit parameters of the EL-QCM are expressed by:

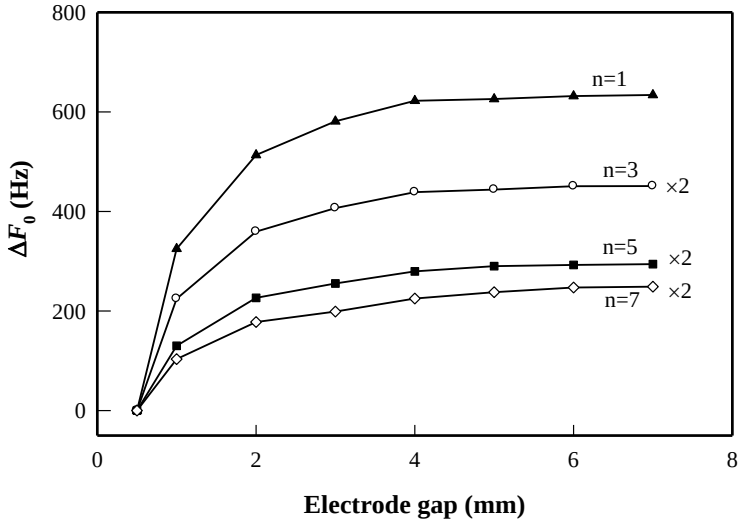

Figure 3. Influence of electrode gap on the resonant frequency of EL-QCM in different overtone .

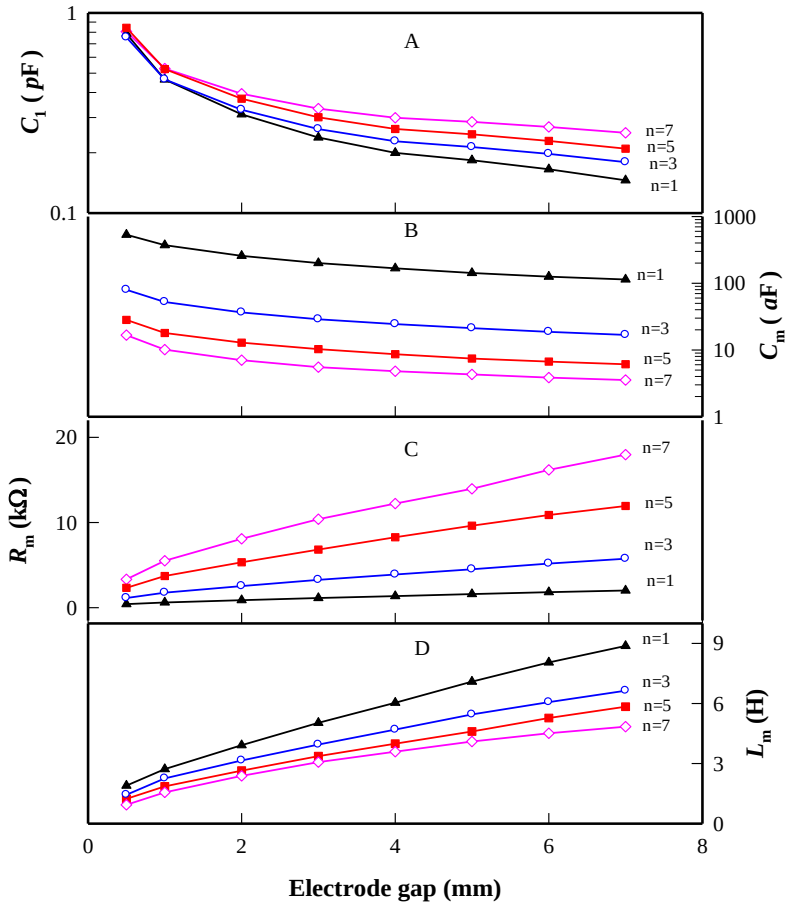

Figure 4. Influence of electrode gap on the equivalent circuit parameters of EL-QCM in different overtone.

$$C_m = \left(\frac{C_{air}}{C_0 + C_{air}} \right)^2 C_q \quad (4)$$

$$L_m = \left(1 + \frac{C_0}{C_{air}} \right)^2 L_q \quad (5)$$

$$R_m = \left(1 + \frac{C_0}{C_{air}} \right)^2 R_q \quad (6)$$

$$C_1 = \frac{C_0 C_{air}}{C_0 + C_{air}} \quad (7)$$

where C_m, L_m, R_m and C_1 are the motional capacitance, motional inductance, motional resistance and static capacitance of the EL-QCM, L_q and R_q the motional inductance and motional resistance of the quartz crystal, respectively.

With increasing electrode gap, the value of C_{air} is reduced, resulting in the decrease in C_m and C_1 as well as the increase in L_m and R_m of the EL-QCM. This prediction is in agreement with the experimental results in all the overtones (n=1,3,5,7). In addition, with increasing overtone number, the values of C_1 and R_m increase but the value of C_m and L_m decrease (Fig.4). For a normal 5MHz QCM in vacuum, the values of R_m and C_m are in linear correlations to n^2 and n^{-2} with the slopes of 0.98 Ω and 26 fF, respectively, and the value of L_m increases slightly with increasing overtone number [29]. According to the data in Fig.4, the values of C_m are in linear correlations to n^{-2} with the slopes decreased from 0.525 to 0.112 fF with increasing electrode gap from 0.5 to 7.0 mm. And values of R_m are also in near-linear correlations to n^2 with the slopes increased from 60 to 328 Ω with increasing electrode gap from 0.5 to 7.0 mm. The difference in the slopes of the plottings of R_m versus n^2 and C_m versus n^{-2} between the EL-QCM and the normal QCM is reasonable because the values of C_m and R_m are related to the electrode gap [24]. Different to the normal QCM, the value of L_m decreases slightly with increasing overtone number. The reason may be that the diameter of the effective vibrating area in the EL-QCM is different slightly to that of the normal QCM.

Under our experimental conditions, there is $C_0 >> C_{air}$ because the higher permittivity and thinner thickness of quartz disc than those of the air layer. According to eqn (7), there is $C_1 \approx C_{air}$. Hence, the static capacitance of the EL-QCM is close to the air capacitance. The increase in C_1 with increasing overtone number maybe due to the increase in across-area of the filed lines passed through the quartz wafer at higher frequency. According to eqn.(4), the reduce in C_1 is ascribed to the remarkable decrease in C_q at higher overtone number. As a result, the value of $f_0 C_q$ in eqn.(3) decreases with increasing overtone number, resulting in the less influence of electrode gap on the resonant frequency at higher overtone number.

Quality factor (Q), defined as the ratio of energy storage to energy loss in a resonator, is an important parameter to evaluate the frequency stability of QCM. The higher of the Q value, the better the frequency stability. For a normal 5MHz QCM in vacuum, the Q factor is 2.25×10^5 [29]. Because the intensity of the resonant peak in EL-QCM is much less than that of the bare quartz resonator itself

due to the high impedance of the air layer, the bypass effect from the static capacitor of EL-QCM is taken into account in the calculation of Q_{eff}, which is expressed by[24]

$$Q_{eff} = \frac{Q}{1+2\pi F_0 R_m C_1} = \frac{2\pi F_0 L_m}{R_m(1+2\pi F_0 R_m C_1)} \qquad (8)$$

As is seen from Fig. 5, the value of Q_{eff} decreases with increasing overtone number. The reason is that the value of L_{m} decreases while value of R_{m} increases at higher overtone. Under our experimental conditions, $Q_{\text{eff}} = 3.8\times10^4$ was measured in the seventh overtone even at the electrode gap of 7 mm. The signal-to-noise ratio of the conductance-frequency curve is still good enough to guarantee a good frequency stability of the EL-QCM in a gaseous phase. Hence, the overtones (n=1,3,5) of EL-QCM were used in the experiments related to bromine adsorption.

3.2 Monitor the adsorption of bromine by EL-QCM

Bromine is a volatile liquid (boiling point 58.8 °C) with high corrosion and toxicity. Our experimental result showed that ZIF-8 has high adsorption capacity to bromine due to its porous structure, offering the potential application in removing Br_2 vapor from gaseous phase. Although QCM is a useful tool to investigate the adsorption kinetics of thin solid films, we failed to monitor the adsorption process of Br_2 vapor by a normal QCM sensor.

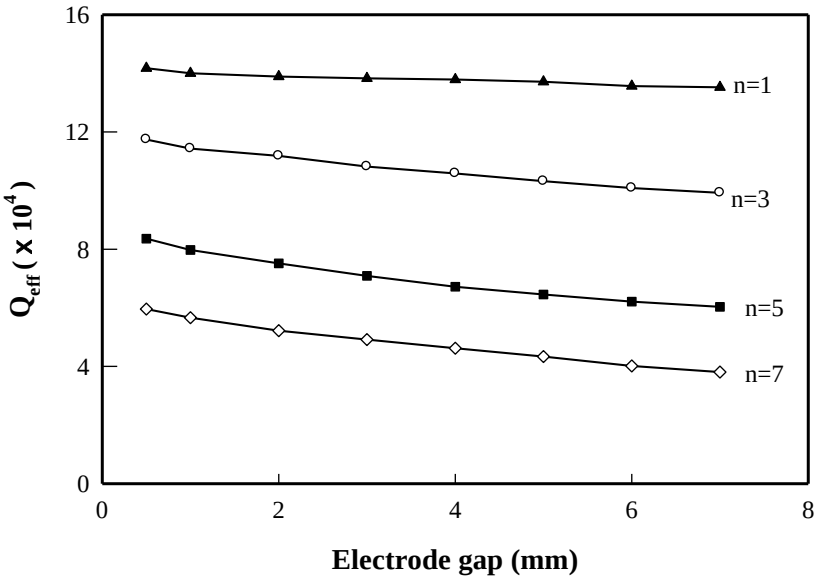

Figure 5. Influence of electrode gap on the effective quality factors of EL-QCM in different overtone.

One reason is that Br_2 can be adsorbed on the surface of Au or Ag electrode on QCM, leading to additional error in amount of Br_2 adsorbed on ZIF-8 film. Another reason is that the joints of the excitation electrodes and leading wires are damaged easily due to the strong corrosion from Br_2. Hence, a purpose-designed EL-QCM (Fig.1B) was employed to monitor the adsorption of Br_2 on ZIF-

8 film. In this experimental setup, ZIF-8 was grown on the surface of bare quartz disc and the electrodes were separated by glass well. Unlike Au electrode, a bare quartz surface has negligible adsorption to Br_2 (data are not shown).

As can be seen in Fig.6, the frequency decreases obviously upon introduction of Br_2 vapor into the cell, indicating a strong adsorption of Br_2 on ZIF-8 film. Under the experimental conditions, the frequency dropped rapidly by 4.53 kHz in the initial 10 min and approach to stable level of -7.1 kHz in 100 min, corresponding an amount of 2.26 g Br_2 adsorbed on per gram of ZIF-8 film. When the cell was vacuumed, an increase in frequency of 1.48 kHz was measured in 30 min, implying that approximately 21% of desorption was taken place. In the control experiment, $ZnNO_3$ and mIm films with similar mass were deposited on the surface of the quartz disc by an electrospraying method. It can be seen that $Zn(NO_3)_2$ film has low adsorption ability to Br_2. The decrease in frequency was only 81 Hz, corresponding to an amount of Br_2 adsorbed of 0.0238g on per gram $Zn(NO_3)_2$. In addition, 81% of Br_2 adsorbed on $Zn(NO_3)_2$ film is reversible in the vacuuming stage. After 100 min, the adsorption of Br_2 on mIm film caused a decrease in frequency of 4.7 kHz, corresponding to an amount of 1.35 g Br_2 adsorbed on per gram of mIm. And about 16% of the adsorption is reversible. This result suggests that the mIm unit play important role for Br_2 adsorption on ZIF-8 film. Importantly, the high surface in ZIF-8 film with porous structure is also advantageous for Br_2 adsorption. The amount of Br_2 adsorbed on ZIF-8 films is 1.67 times of that on mIm film. For adsorption on Au film deposited on the surface of quartz wafer by a plasma spraying method, the decrease in frequency was 3.19 kHz in 100 min, corresponding to a Br_2 layer with thickness of 0.182 μm. In the desorption stage, 9% of Br_2 adsorbed on Au surface is desorbed, revealing that most of Br_2 was adsorbed chemically on Au film.

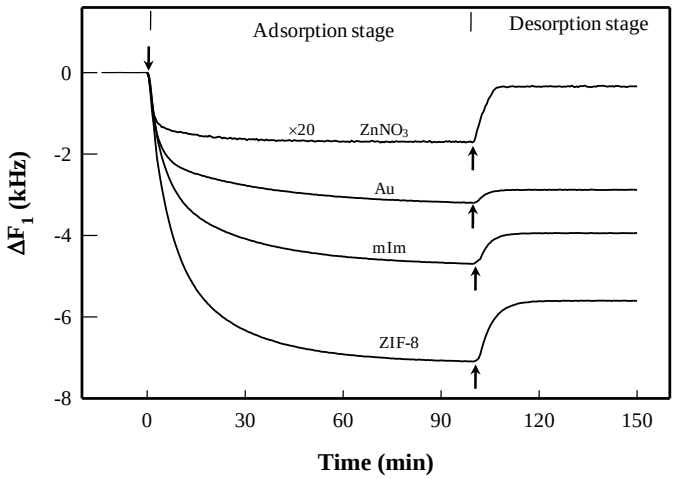

Figure 6. Shifts of the resonant frequency of EL-QCM (n=1) during the adsorption and desorption stages. The downward arrow indicates the addition of 3.5 mg/L Br_2 and the upward arrows indicate the start of desorption by vacuumizing operation. The frequency shifts of -3.40, -2.52, -3.48 and -3.14 kHz were measured with the of $Zn(NO_3)_2$, Au, mIm and ZIF-8 films deposited, respectively.

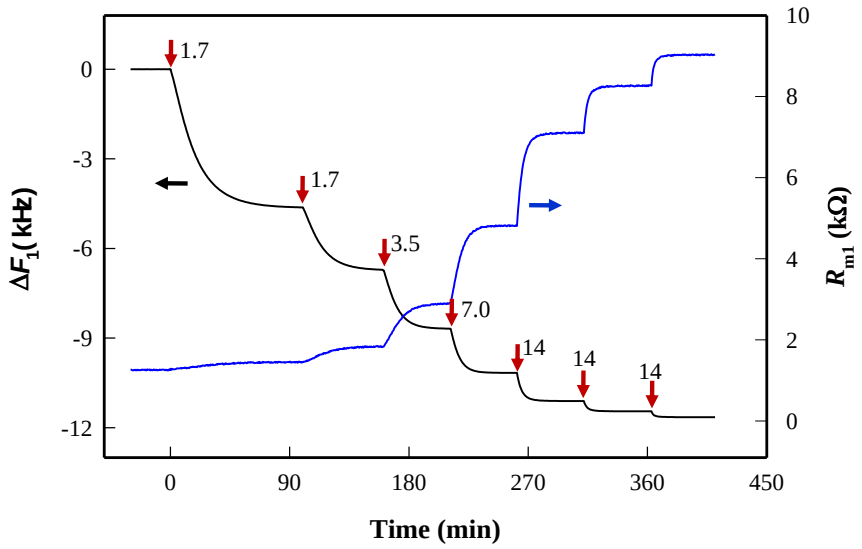

Figure 7. Shifts of the resonant frequency and motional resistance of EL-QCM (n=1) during a sequential adsorption. The downward arrows indicates the addition of Br_2 in mg/L. The thickness of ZIF-8 film was 0.68μm.

Fig.7 depicts the changes in frequency and motional resistance of the EL-QCM during an adsorption process in sequential addition of Br_2. In the initial addition of 1.7 mg/L Br_2, the frequency decreases 4.6 kHz while the motional resistance increases from 1.27 to 1.45 kΩ in 100 min. The small change in motional resistance reveals that the rigidity of the film is hardly influenced by the adsorption of Br_2 at low concentration. In the second addition of 1.7 mg/L Br_2, a further decrease in frequency of 2.1 kHz was measured in 50 min. Note that the motional resistance was increased from 1.45 to 1.84 kΩ in this stage, implying the rigidity of the film was reduced slightly. As part of the sites were occupied further, the frequency shift in the sequential addition of Br_2 stage was reduced and approached to zero in the last stage. But the increase in the motional resistance is speeded up with respect to the same frequency shift, especially in the last adsorption stage. A larger motional resistance means a larger energy loss in the resonance of the QCM, which reveals the decrease in the rigidity of the film with Br_2 adsorbed. As a result, the validity of the Sauerbrey relation may be questionable in the case of heavy energy loss from the film.

It is well known that the response of a QCM in a liquid phase is related to both of the mass and non-mass effects [30]. The frequency shift due to the non-mass effect, such as the viscosity, density and conductivity of the liquid phase, leads to the error in estimation of the mass change by using the Sauerbrey equation [31]. To extract reliable mass change information from the QCM in liquid phase, the correlations of the frequency shift and equivalent circuit parameters were reported [32-37]. On the other hand, it is often informative to compare the changes in frequency from different overtones in QCM with dissipation (QCM-D) since the propagation of the crystals resonance energy into the adsorbed layer and surrounding liquid is sensitive to the viscoelastic properties of the layer [38]. A homogeneous, rigid layer will damp the resonance overtones proportionally to the same extent, in which case the change in normalised frequency ($\Delta F_n/n$) will be the same for each overtone. For a low

viscosity, liquid-like layer, however, the propagation of the crystals' resonance will vary with overtone number with the penetration depth decreasing with increasing overtone number [39-42]. As viscosity and density of a gaseous phase are much less than those of a liquid phase, the energy loss from the surface of oscillating quartz wafer to the gaseous phase in EL-QCM is neglectable. Hence, it is reasonable to assume the increase in motional resistance (Fig.7) is due to the less rigid film after Br_2 adsorption.

To further investigate the influence of Br_2 adsorption on the rigidity of ZIF-8 film, the overtone response of the EL-QCM with film thickness of 0.366, 0.691 and 1.18 μm were measured. In the case with h=0.366 μm, the ratios of the frequency shifts in the third and fifth overtones to fundamental frequency shift, ($\Delta F_{03}/\Delta F_{01}$) and ($\Delta F_{05}/\Delta F_{01}$), were estimated to be 3.001 and 5.003, respectively (data are not shown). This result suggests that the rigidity of ZIF-8 film is not varied obviously in low amount of Br_2 added, which is supported by the motional resistance of the EL-QCM. As is seen in Fig.8A, the motional resistance is increased from 1.18 to 1.73 kΩ with the total frequency shift of -6.9 kHz. The negligibly small change in motional resistance indicates that the Sauerbrey equation is valid and hence the adsorbed mass can be calculated from eqn.(1). The frequency shift of -6.9 kHz is corresponded to the saturated adsorption capacity 3.52 g per gram ZIF-8, or the amount of Br_2 adsorbed of 123 μg/cm^2.

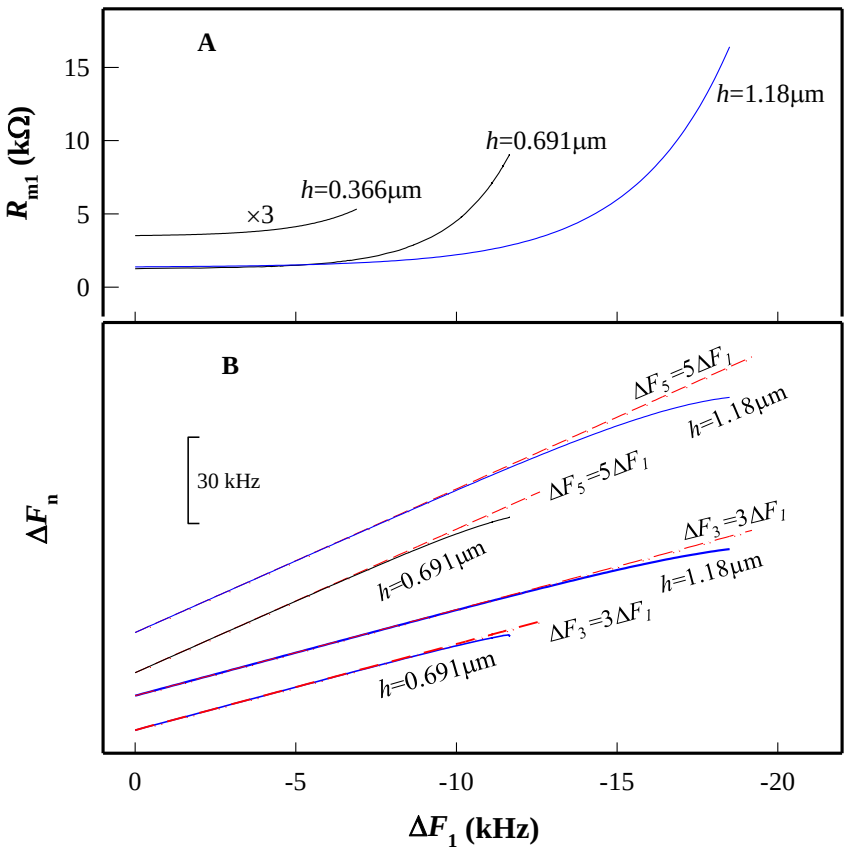

Figure 8. Motional resistance versus frequency shifts (n=1) (A) and the correlations of the frequency shifts in overtone (n=1,3,5) (B) of EL-QCM during the adsorption of Br_2 on ZIF-8 film of different thickness. The curves in (B) were shifted vertically for clarity and the dashed lines (red) indicates the theoretical correlations.

By using the density of 3.12 g/mL, the amount of Br_2 adsorbed is equivalent to a thickness of 0.39 μm, indicating that Br_2 was adsorbed in the cavities and surface of ZIF-8 film.

Fig. 8B compares the plots of ΔF_{03} versus ΔF_{01} and ΔF_{05} versus ΔF_{01} in EL-QCM with ZIF-8 film of 0.691 and 1.18 μm during Br_2 adsorption. The experimental curves are deviated from the theoretical lines in the late adsorption stage, especially in the case of h=1.18 μm. The reason is that the ZIF-8 film may be softened with high amount of Br_2 adsorbed, supporting by the steep increase in motional resistance with increasing frequency shifts in the late adsorption stage (Fig.8A). In the case of h=1.18 μm, for example, the motional resistance is increased from 1.39 to 3.04 kΩ in the linear region with a frequency shift of -11.7 kHz. But it is increased from 3.04 to 16.4 kΩ in the deviation area with frequency shift decreased further from -11.7 to -18.5 kHz. Such frequency shifts are equivalent to the thickness of pure Br_2 layer adsorbed on ZIF-8 film approximately in the range from 0.67 to 1.06 μm. With Br_2 adsorbed in the cavities of ZIF-8 film, they damp the resonance overtones proportionally to nearly the same extent like in the case of rigid film. For Br_2 adsorbed on the surface of ZIF-8 film, they show decreasing mass loading impact with increasing overtone, although the thickness may be in the penetration depth of the QCM. Hence, the deviation of the experimental curves from theoretical lines is slight under our experimental conditions, especially in the case of thinner film layer.

3.3 Measurement of adsorption thermodynamic and kinetical parameters

In this experimental, ZIF-8 films with thickness of 0.65 ± 0.01 μm were grown on the surface of quartz crystal for Br_2 adsorption and the shift in the fundamental frequency was recorded to estimate the amount of Br_2 adsorbed according to Sauerbrey relation. Fig.9A depicts the adsorption isotherms of Br_2 onto ZIF-8 film at the temperature of 25, 40 and 60 °C. The concentration of the Br_2 in the cell is assumed to be close to the amount added for simplification the data analysis. The isotherm data were treated according to the well-known Langmuir and Freundlich isotherm models, which are formulated as

$$\Gamma_e = \frac{\Gamma_{max} K_L C_e}{1 + K_L C_e} \quad (9)$$

$$\Gamma_e = K_F C_e^{1/n} \quad (10)$$

where Γ_{max} (mg/g) and K_L (L/g) are the saturation adsorption capacity and adsorption equilibrium constant in Langmuir model, K_F and $1/n$ are Freundlich constants, respectively, C_e is the equilibrium concentration of Br_2 in cell (mg/L).

The fitting constants in the Langmuir and Freundlich models are listed in Table 1. Under the experimental conditions used, the Langmuir model was found to represent the equilibrium data with a much better fit as compared to the Freundlich model. The values of Γ_{max} and K_L decrease with increasing temperature (20~60°C). The reason may be that the amounts of Br_2 in physical adsorption are reduced at higher temperature due to the volatility of Br_2. As shown in Fig.9B, the percent of the reversible adsorption to total adsorption, Γ_r/Γ, is reduced also with increasing temperature. On the other hand, with increasing Br_2 concentration, the value of Γ_r/Γ increases, implying that more Br_2 molecules are adsorbed on the surface in physical adsorption mechanism.

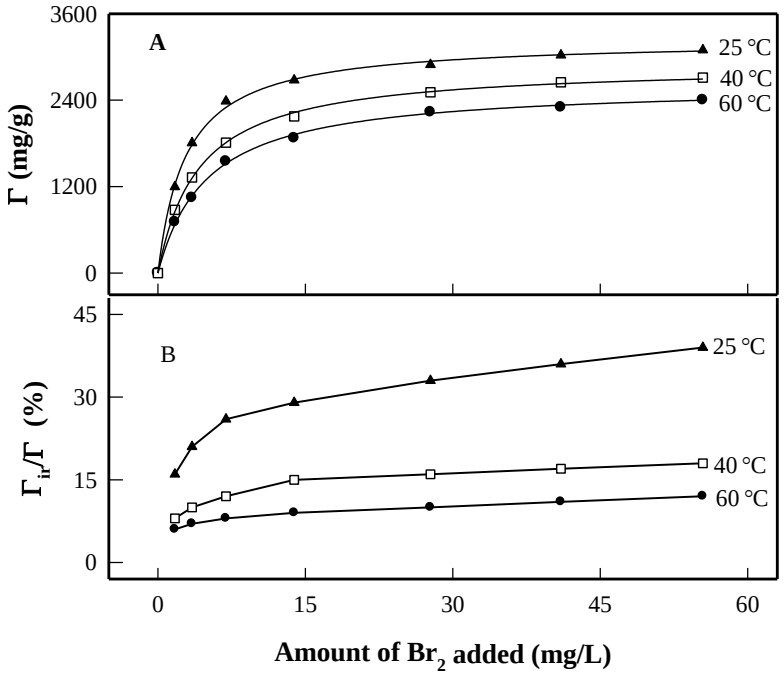

Figure 9. Adsorption isotherms o f Br_2 on ZIF-8 film at different temperature. The thickness of ZIF-8 film was 0.65 ± 0.01 μm.

Table 1. Fitting constants and coefficients of correlation (r^2) for Langmuir and Freundlich equations to the experimental data for Br_2 adsorption on ZIF-8 films with thickness of 0.65±0.01 μm.

	Langmuir model			Freundlich model		
T °C	Γ_{max} mg/g	K_L L/g	r^2	K_F	*1/n*	r^2
25	3241	352.7	0.9983	9127	0.279	0.9362
40	2893	241.3	0.9931	8220	0.351	0.9463
60	1616	200.6	0.9918	5687	0.389	0.9586

In addition, the adsorption kinetic curves are well fitted by the pseudo-second-order kinetic model, which is expressed by [43]

$$\frac{t}{\Gamma_t} = \frac{1}{k_2 \Gamma_e^2} + \frac{t}{\Gamma_e} \qquad (11)$$

where Γ_t and Γ_e are the amounts adsorbed at time of *t* and adsorption equilibrium, k_2 is the rate constant of pseudo-second-order model. The reciprocal of the intercept in eqn.(11) is defined as the initial rate of adsorption ($V_0 = k_2 Q_e^2$).

Table 2. The fitting parameter in pseudo-second-order model for the adsorption of Br_2 on ZIF-8 films with a thickness of 0.65±0.01 μm.

C mg/L	T °C	k_2 $mg.g^{-1}.min^{-1}$	Γ_e $mg.g^{-1}$	r^2	V_0 $mg.g^{-1}.min^{-1}$	E_a kJ/mol
3.50	25	2.12×10^{-5}	1781	0.9932	67.5	35.3
	40	4.93×10^{-5}	1318	0.9968	85.5	
	60	9.56×10^{-5}	1071	0.9986	109	
14.0	25	3.65×10^{-5}	2696	0.9948	265	27.6
	40	7.05×10^{-5}	2236	0.9971	352	
	60	1.17×10^{-4}	1930	0.9988	436	
35.0	25	7.16×10^{-5}	2997	0.9946	643	22.8
	40	1.17×10^{-4}	2587	0.9981	786	
	60	1.83×10^{-4}	2289	0.9990	958	

As listed in Table 2, the rate constant and initial adsorption rate increase with increasing temperature and the concentration of Br_2 vapor. The dependence of adsorption rate constant on temperature can be used to estimate adsorption activation energy (E_a) according to the Arrhenius's equation [44]:

$$\ln k = \ln A_0 - \frac{E_a}{RT} \qquad (12)$$

where A_0 is a constant called the frequency factor, R is the universal gas constant, T is the temperature in Kelvin. Consequently, when ln$k$ is plotted versus 1/T, a straight line with slope -E_a/R is obtained. Under the experimental conditions used, the values of E_a are 35.3, 27.6 and 22.8 kJ/mol for the adsorption at the Br_2 concentration of 3.50,14.0 and 35.0 mg/L, respectively.

4. CONCLUSION

This work demonstrates that the overtones in an EL-QCM has high quality factor and excellent frequency stability. With increasing overtone number, the influence of electrode gap on the resonant frequency is reduced due to the improvement in the conductance of the air layer at higher frequency. On the other hand, with increasing overtone number, the static capacitance and motional resistance increase while the motional capacitance, motional inductance and quality factor decrease. In the application of EL-QCM to monitor the adsorption of Br_2 vapor on ZIF-8 film, the correlations of the frequency shifts in overtone can be also used to judge the rigidity of the film. For adsorption on a thin ZIF-8 film (0.366 μm), the normalised frequency (ΔF_n/n) is very close for each overtone and the

change in motional resistance is slight, implying that the rigidity of the film is hardly influenced by the Br_2 adsorbed layer and the Sauerbrey equation is valid in estimation the adsorbed mass. The adsorption isotherm follows Langmuir model with a saturation adsorption capacity of 3.52 g per gram ZIF-8 (25°C). The adsorption kinetics obeys the pseudo-second-order model. For adsorption on a thick ZIF-8 film (1.18 μm), the plots of ΔF_{03} versus ΔF_{01} and ΔF_{05} versus ΔF_{01} are deviated from the theoretical lines in the late adsorption stage, in which the motional resistance is increased steeply, indicating the decrease in rigidity of the film. With Br_2 adsorbed in the cavities of ZIF-8 film, they damp the resonance overtones proportionally to nearly the same extent like in the case of rigid film. For Br_2 adsorbed on the surface of ZIF-8 film, they show decreasing mass loading impact with increasing overtone. Hence, the deviation of the experimental curves from theoretical lines is slight under our experimental conditions, especially in the case of thinner film layer. The adsorption of Br_2 on ZIF-8 film demonstrates the applicability of EL-QCM in gaseous phase, offering the advantages over normal QCM in optical transparency, longer lifetime, better experimental reproducibility, reduced number of preparation steps and lower costs.

ACKNOWLEDGEMENTS
The authors gratefully acknowledge financial support of National Natural Science Foundation of China (21175084, 21275091, 21575080).

References

1. Q. Chen, X.J. Wu, D.Z. Wang, W. Tang, N. Li and F. Liu, *Analyst*, 136(2011)2572.
2. A. R. Hillman, "The Electrochemical Quartz Crystal Microbalance" in Encyclopedia of Electrochemistry, A. J. Bard and M. Stratmann (Series eds.); Wiley-VCH, Weinheim, 2003, Vol. 3, P. R. Unwin (Vol. ed.), pp. 230-289.
3. J. John, K. M. Hugar, J. Rivera-Melé ndez, H. A. Kostalik, IV, E. D. Rus, H. Wang, G.W. Coates and H. D. Abruña, *J. Am. Chem. Soc.*, 136(2013)5309.
4. *L.S. Liu*, *J.M. Kim* and *W.S. Kim*, *Anal. Chem.*, 87(2015)3329.
5. Q. Chen, S.M. Xu，Q.X.Liu, J. Masliyah and Z.H. Xu, *Adv. Colloid Interface Sci.*, 2016, http://dx.doi.org/10.1016/ j.cis.2015. 10.004.
6. K.A. Marx, *Biomacromolecules*, 4(2003)1099.
7. S.Z. Yao, Piezoelectric Chemistry and Biosensors. Chemical Industry Press, Beijing, 2006.
8. G.N.M. Ferreira, A.C. da-Silva and B. Tomé, *Trends Biotechnol.*, 27(2009)689.
9. 9.. Z.B. Chen, J.H. Wu, Y. Zhao, F. Xu and Y.Q. Hu, *Anal. Methods*, 4(2012)599.
10. C. I. Cheng, Y.P. Chang and Y.H. Chu, *Chem. Soc. Rev*., 41(2012)1947.
11. Q.J. Liu, C.S. Wu, H. Cai, N. Hu, J. Zhou and P. Wang, *Chem. Rev*.,114(2014)6423.
12. G. Sauerbrey, *Z. Phys.*, 155(1959)206.
13. H. Ogi, H. Naga,Y. Fukunishi, M. Hirao and M. Nishiyama, *Anal. Chem.*, 81(2009)8068.
14. Z.H. Mo, L.H. Nie and S.Z. Yao, *J. Electroanal. Chem.*, 316 (1991)79.
15. T. Nomura, F. Tanaka, T. Yamada and H. Itoh, *Anal. Chim. Acta*, 243(1991)273.
16. J.T. Hu, D.L. Yang, Q. Kang and D.Z. Shen, *Sens. Actuators B*, 96(2003)390.
17. H. Ogi, Y. Fukunishi, H. Nagai, K. Okamoto,M. Hirao and M. Nishiyam, *Biosens. Bioelectron.*, 24(2009)3148.
18. Q. Kang, R. Sheng, Y.L.Li, Z.L.Zhang, S.J.Wu and D.Z. Shen, *Sens. Actuators B*, 157(2011)533.
19. A. Kunze, M. Zäch, S. Svedhem and B. Kasemo, *Biosens. Bioelectron.*, 26(2011)1833.
20. H.Ogi,K. Motoshisa, T. Matsumoto, K. Hatanaka and M. Hirao, *Anal. Chem.*, 78(2006)6903.

21. H. Ogi, H. Nagai, Y. Fukunishi, T. Yanagida, M. Hirao and M. Nishiyama, *Anal. Chem.*, 82(2010) 3957.
22. H. Ogi, T. Yanagida, M. Hirao and M. Nishiyama, *Biosens. Bioelectron.*, 26(2011)4819.
23. W. Ko and S. Jeon, *Sens. Actuators B*, 193(2014)774.
24. Q. Kang, X.L. Zhu, X.L. Ma, L.Q. Kong, W.T. Xu and D.Z. Shen, *Sens. Actuators B*, 220(2015)472.
25. D. F. Sava,M. A. Rodriguez,K W. Chapman,P J. Chupas,J A. Greathouse,P S. Crozier and T. M. Nenoff, *J. Am. Chem. Soc*., 133(2011)12398.
26. J.T. Hughes,D. F. Sava,T. M. Nenoff and A. Navrotsky, *J. Am. Chem. Soc.*, 135(2013)1625.
27. Q. Kang, Y. Qi, P. Zhang and D.Z. Shen, *Talanta*, 72 (2007)1474.
28. S. N. Wijenayake, N. P. Panapitiya, S. H. Versteeg, C. N. Nguyen, S. Goel,K. J. Balkus, Jr., I. H. Musselman and J. P. Ferraris, *Ind. Eng. Chem. Res.*, 52(2013)6991.
29. M. Cassiède, J.H. Paillol, J. Pauly, J.L. Daridon, *Sen. Actuators A*, 159 (2010) 174–183.
30. M. Thompson, A.L. Kipling, W.C. Duncan-Hewitt, L.V. Rajakovic and B.A. CavicVlasak, *Analyst*, 116 (1991)881.
31. V.M. Mecea, *Sen. Actuators A*, 128(2006)270.
32. H. Muramatsu, E. Tamiya and I. Karube, *Anal. Chem.*, 60(1988)2142.
33. M. Yang and M. Thompson, *Anal. Chem.*, 65(1993)1158.
34. Q. Xie, J. Wang, A. Zhou, Y. Zhang, H. Liu, Z. Xu, Y. Yuan, M. Deng and S. Yao, *Anal. Chem.*, 71(1999)4649.
35. M. Cassiède, J.L. Daridon, J.H. Paillol and J. Pauly, *Sens. Actuators A*, 167(2011)317.
36. D.Z. Shen, X.L. Ma, T.T. Cai, X.L. Zhu, X.D. Xin and Q. Kang, *Anal. Methods*, 7(2015) 9619.
37. A. R. Patel, K. K. Kanazawa and C. W. Frank, *Anal. Chem*., 81(2009)6021.
38. A. A. Feiler, A. Sahlholm, T. Sandberg and K. D. Caldwell, *J. Colloid Interface Sci.*, 315(2007)475.
39. Y.Z. Zhang,B.Y. Du, X.N. Chen and H.W. Ma, *Anal. Chem.*, 81(2009)642.
40. S. V. Orski, S. Kundu,R Gross and K. L. Beers, *Biomacromolecules*,14(2013)377.
41. L. Sun,S. Svedhem and B. Åkerman, *Langmuir*, 30(2014)8432.
42. S.L. Zhang, H.H. Bai and P.H. Yang, *Chem. Commun.*, 51(2015)11449.
43. G. McKay and Y. S. Ho, *Process Biochem.*, 34(1999)451.
44. Y. Sağ and T. Kutsal, *Process Biochem.*, 35(2000)801.